Description of the Behaviour of Cellular Composite with Weak Filling Material

E. Postek and T. Sadowski

Abstract The aim of this presentation is to show the behaviour of a cellular composite material. The material is two-phase consisting of metallic, relatively rigid interfaces and weak filling material. Such type of a generic composite is used as core filler between external layers of sandwich composite material applied in aerospace engineering. We investigate the limit load of a sample varying the initial void ratio in the filling. We are using the Tvergaard-Gurson in order to describe porosity existence in the material and elasto-plastic models with the assumption of presence of the finite deformations. The geometrical model is three-dimensional.

1 Introduction

A generic model of a two-phase composite is presented. This model can be used for an analysis of a cellular composite with weak filling material. The initial porosities can be as high as 60%. The problem is highly non-linear because of initial stress stiffness, plasticity and possibly voids nucleation. In our case we follow the analysis up to appearance of plastic strain which develops close to junctions of the stiff skeleton and close to surfaces where the pressure is applied.

E. Postek (✉)
School of Earth and Environment, Institute of Geophysics and Tectonics, University of Leeds, Woodhouse Lane, Leeds, LS2 9JT, UK
e.w.postek@leeds.ac.uk

T. Sadowski
Faculty of Civil and Sanitary Engineering, Department of Solid Mechanics, Lublin University of Technology, ul. Nadbystrzycka 40, 20-618 Lublin, Poland
tsadow@akropolis.pol.lublin.pl

2 Formulation

2.1 Incremental Equation of Equilibrium

The problem is elasto-plastic with the assumption of large displacements [1–3]. We
consider nonlinear terms of the strain tensor. The virtual work equation is of the form

$$\delta\Pi = \int_{\Omega^o}^{t+\Delta t} {}_oS \cdot \delta^{t+\Delta t}{}_oE d\Omega^o - \int_{\Omega^o} {}^{t+\Delta t}f\delta^{t+\Delta t}u d\Omega^o - \int_{\partial\Omega_\sigma^o} {}^{t+\Delta t}t\delta^{t+\Delta t}u d\left(\partial\Omega_\sigma^o\right), \quad (1)$$

where S and E are the second Piola-Kirchhof stress tensor and Green Lagrange
strains, f, t and $u = \{u, v, w\}$ are body forces, boundary tractions and displacements.
All of the quantities are determined at time $t + \Delta t$ in the initial configuration. To
obtain the above equation at time $t + \Delta t$ in the configuration at time t the relations
[4, 5], are used

$$^{t+\Delta t}{}_oS = \frac{\rho}{\rho_o}{}^{t+\Delta t}{}_tS, \quad ^{t+\Delta t}{}_oE = \frac{\rho}{\rho_o}{}^{t+\Delta t}{}_tE, \quad \rho d\Omega^t = \rho_o \, d\Omega^o \quad (2)$$

$$\int_{\Omega^t} {}^{t+\Delta t}{}_tS \cdot \delta^{t+\Delta t}{}_tE \, d\Omega^t = \int_{\Omega^t} {}^{t+\Delta t}t\delta^{t+\Delta t}u \, d\Omega^t + \int_{\partial\Omega_\sigma^t} {}^{t+\Delta t}t\delta^{t+\Delta t}u \, d\left(\partial\Omega_\sigma^t\right). \quad (3)$$

Now, we apply incremental decomposition to the quantities in the equation above:
strains, stresses, displacements and forces

$$^{t+\Delta t}{}_tE = {}^t_tE + \Delta E, \; ^{t+\Delta t}{}_tS = {}^t_tS + \Delta S, ^{t+\Delta t}u = {}^tu + \Delta u, \; ^{t+\Delta t}f = {}^tf + \Delta S. \quad (4)$$

Since the second Piola-Kirchhoff tensor at time t in the configuration t is equal to
the Cauchy stress tensor the stress decomposition is of the form
$^t_tS = {}^t_t\tau$ and $^{t+\Delta t}{}_tS = {}^t_t\tau + \Delta S$. Then, we employ the following strain increment
decomposition into its linear and nonlinear parts in the following form $\Delta E =
\Delta e + \Delta\eta$, $\Delta e = \bar{A}\Delta u$ and $\Delta\eta = \bar{\bar{A}}(\Delta u')\Delta u'/2$ where $\Delta u'$ is the vector of the dis-
placement increment derivatives w.r.t. Cartesian coordinates and $\bar{A}, \bar{\bar{A}}$ are the linear
and nonlinear operators [2]. The operators act on linear and nonlinear parts of the
strain tensor.

Substituting the described relations, into the virtual work equation, Eq. (3), and
assuming that the equation is precisely fulfilled at the end of the step we obtain the
following incremental form of the virtual work equation.

$$\int_{\Omega^t} \left({}^t_t\tau \cdot \delta\eta + \Delta S \cdot \delta\Delta e\right) \, d\Omega^t = \int_{\Omega^t} \Delta f \, \delta\Delta u d\Omega^t + \int_{\partial\Omega_\sigma^t} \Delta t \, \delta\Delta u \, d\left(\partial\Omega_\sigma^t\right). \quad (5)$$

Employing the finite element approximation $\Delta\mathbf{u} = \mathbf{N}\Delta\mathbf{q}$ and $\Delta\mathbf{u}' = \mathbf{B}'\Delta\mathbf{q}$ where $\mathbf{N}$ is the set of shape functions and $\Delta\mathbf{q}$ is the increment of nodal displacements and considering the following set of equalities

$$
{}_t^t\boldsymbol{\tau}^{\mathrm{T}}\delta\eta = {}_t^t\boldsymbol{\tau}\delta\left(\bar{\bar{\mathbf{A}}}\right)\Delta\mathbf{u}' = \delta\left(\Delta\mathbf{u}'\right)^{\mathrm{T}}{}_t^t\bar{\boldsymbol{\tau}}\,\Delta\mathbf{u}' = \delta\left(\Delta\mathbf{q}\right)^{\mathrm{T}}{}_t^t\bar{\boldsymbol{\tau}}\,\mathbf{B}'_L, \tag{6}
$$

where ${}_t^t\bar{\boldsymbol{\tau}}$ is the Cauchy stress matrix

$$
{}_t^t\bar{\boldsymbol{\tau}} = \begin{bmatrix} {}_t^t\underline{\boldsymbol{\tau}} & & \\ & {}_t^t\underline{\boldsymbol{\tau}} & \\ & & {}_t^t\underline{\boldsymbol{\tau}} \end{bmatrix} \qquad {}_t^t\underline{\boldsymbol{\tau}} = \begin{bmatrix} {}_t^t\sigma_{xx} & {}_t^t\tau_{xy} & {}_t^t\tau_{xz} \\ & {}_t^t\sigma_{yy} & \tau_{yz} \\ & & {}_t^t\sigma_{zz} \end{bmatrix}, \tag{7}
$$

we obtain the following discretized form of the virtual work equation

$$
\left(\int_{\Omega^t}\mathbf{B}'_L{}^{\mathrm{T}}{}_t^t\bar{\boldsymbol{\tau}}\mathbf{B}'_L\,d\Omega^t\right)\Delta\mathbf{q} + \int_{\Omega^t}\mathbf{B}_L^{\mathrm{T}}\Delta\mathbf{S}\,d\Omega^t = \int_{\Omega^t}\mathbf{N}^{\mathrm{T}}\Delta\mathbf{f}\,d\Omega^t + \int_{\partial\Omega^t_\sigma}\mathbf{N}^{\mathrm{T}}\Delta\mathbf{t}\,d\left(\partial\Omega^t_\sigma\right). \tag{8}
$$

Now, we will deal with the constitutive model and employ the linearized constitutive equation, in fact with the stress increment, $\Delta\mathbf{S}$.

2.2 Finite Strains

When considering the finite strains effect [6, 7], the gradient $\mathbf{F} = \partial\left(\mathbf{X}+\mathbf{u}\right)/\partial\mathbf{x}$ is decomposed into its elastic and plastic parts, $\mathbf{F} = \mathbf{F}^e\mathbf{F}^p$. To integrate the constitutive relations the deformation increment $\Delta\mathbf{D}$ is rotated to the un-rotated configuration by means of rotation matrix obtained from polar decomposition $\mathbf{F} = \mathbf{V}\mathbf{R} = \mathbf{R}\mathbf{U}$, $\Delta\mathbf{d} = \mathbf{R}_{n+1}^T\Delta\mathbf{D}\mathbf{R}_{n+1}$, then the radial return is performed and stresses are transformed to the Cauchy stresses at $n+1$, $\sigma_{n+1} = \mathbf{R}_{n+1}\sigma_{n+1}^u\mathbf{R}_{n+1}^T$. The stresses are integrated using the consistent tangent matrix [8] and the integration is done in the un-rotated configuration as for small strains.

3 Constitutive Model

The constitutive model is the Gurson Tvergaard model [9–11] with the yield function as follows

$$
F = \left(\frac{\sigma^M}{\bar{\sigma}}\right)^2 + 2q_1 f\cosh\left(\frac{3q_2\sigma_m}{2\bar{\sigma}}\right) - \left(1 + q_3 f^2\right), \tag{9}
$$

where σ^M is the Mises stress, σ_m is the mean stress, $\bar{\sigma}$ is the Mises stress in the matrix, f is the void ratio and $q_1, q_2\ q_3$ are the Tvergaard coefficients.

The stress integration algorithm comprises the elastic trial stress (predictor) and the corrector. It conforms the radial return algorithm. The algorithm can be derived basing on [12]. The elastic trial stress are of the form

$$\sigma^E_{m+1} = \sigma_m + \mathbf{D}\,\Delta\varepsilon^{pl}. \tag{10}$$

The deviatioric and the volumetric stress are of the form

$$q_{m+1} = \sqrt{\left(\frac{3}{2}S_{ij}S_{ij}\right)_{m+1}} \qquad p_{m+1} = -\frac{1}{3}(\sigma_{11} + \sigma_{22} + \sigma_{33})_{m+1}. \tag{11}$$

The increment of the plastic strains can be obtained from the normality condition.

$$d\varepsilon^{pl} = d\lambda\frac{\partial F}{\partial\sigma} \tag{12}$$

Further, the plastic strains increment and the unit normal vector are of the form

$$\Delta\varepsilon^{pl} = \Delta\lambda\left(-\frac{1}{3}\frac{\partial F}{\partial p}\mathbf{I} + \frac{\partial F}{\partial q}\mathbf{n}\right)_{m+1} \qquad \mathbf{n}_{m+1} = \frac{3}{2q_{m+1}}\mathbf{S}_{m+1}. \tag{13}$$

The stress at the end of the $(m+1)$ takes the form

$$\sigma_{m+1} = \sigma^E - \mathbf{D}\Delta\varepsilon^{pl}. \tag{14}$$

Since the increment of plastic strains is

$$\Delta\varepsilon^{pl} = \frac{1}{3}\Delta\varepsilon_p\mathbf{I} + \Delta\varepsilon_q\mathbf{n}_{m+1}, \tag{15}$$

the stress at the end of the step may be expressed as follows

$$\sigma_{m+1} = \sigma^E_{m+1} - K\Delta\varepsilon_p\mathbf{I} - 2G\Delta\varepsilon_q\mathbf{n}_{m+1}. \tag{16}$$

The updated stresses are of the form

$$\sigma_{m+1} = \sigma^E_{m+1} - K\Delta\varepsilon_p\mathbf{I} - \frac{3G\Delta\varepsilon_q}{q^T_{m+1}}\mathbf{S}^E_{m+1}, \tag{17}$$

where the quantities designated with the index (E) are the elastic trial stresses.

4 Numerical Example

We consider two cases of the material of the different Young's moduli of the filling material. The Young's moduli are $0.2E + 11 \, \text{N/m}^2$ and much lower $0.005E + 11 \, \text{N/m}^2$. Both moduli significantly lower the Young's modulus of the skeleton which is $2.1E + 11 \, \text{N/m}^2$. The yield limits are $15.0E + 6$ and $297.0E + 6 \, \text{N/m}^2$. The initial porosity of the filler is 0.3. We observe the most characteristic features of the behaviour of the material. Our interest is focused on the vertical displacements, equivalent total strains, plastic strains and Mises stress.

Observing all figures (Figs. 1–4) we may notice qualitatively different performance of both materials. The vertical z-displacements (Fig. 1) is more equally distributed and is lower, 0.725E-5 mm, in the case A than in the case B, 0.358E-3 m. This z-displacements distribution gives a picture of roughness of the material during loading. The weaker sample becomes thinner close to the loaded edge. When concerning the total equivalent strain (Fig. 2) we may notice higher contrasts in the case of stronger material. The strain is distinctly lower in all interfaces than in the cells. The maximum strain, 0.691E-3 is lower than in the case of the weaker material, 0.418E-1.

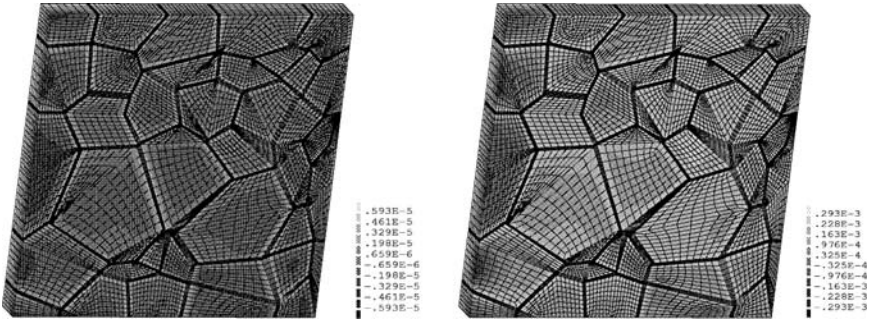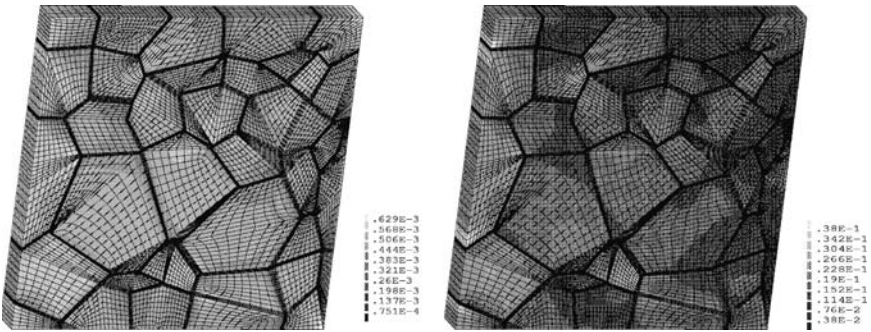**Fig. 1** Veritical displacements distributions (cases A and B)

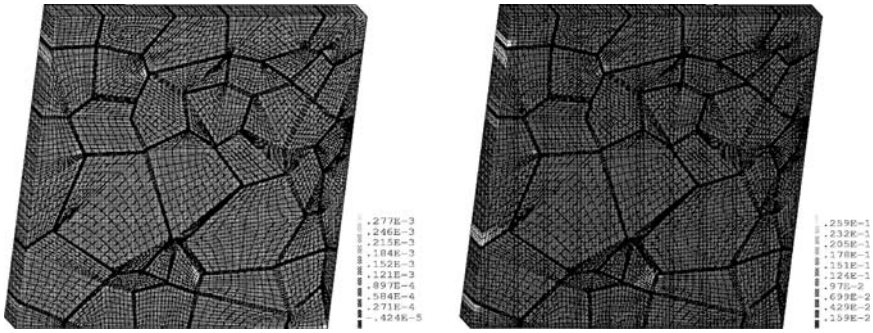**Fig. 2** Equivalent strain distribution (cases A and B)

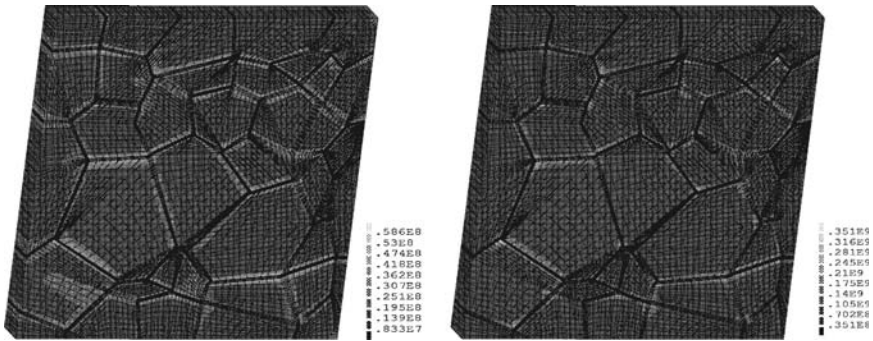**Fig. 3** Equivalent plastic strain distribution (cases A and B)

Fig. 4 Mises stress distribution (cases A and B)

The equivalent plastic strain distribution (Fig. 3) is different in both cases. In the case of stronger material there are more equivalent plastic spots within the sample than in the case of weaker material. The plastic strain are more localized in the weaker sample. The equivalent plastic strain reads 0.309E-3 and 0.286E-1, respectively.

The Mises stress distributions are presented in Fig. 4. The Mises stress is the highest in the junctions of the skeleton and in the edges of the skeleton. The maximum stress is higher in the sample with weaker filling material $(0.386E + 9\,Pa)$ than in the case of stiffer sample $(0.642E + 8\,Pa)$. The stress contrasts are higher in the case of weaker sample.

The calculations were performed for the same load level, $80.4E + 6\,Pa$.

5   Final Remark

A generic numerical model of a material with weak filling material is presented. The weak material is modelled using Tvergaard Gurson material. This approach is convenient and allows to model material with high initial volume of voids.

References

1. Owen, D.R.J., Hinton, E. (1980) Finite Elements in Plasticity: Theory and Practice, Pineridge, Swansea, UK.
2. Bathe, K.J. (1996) Finite Element Procedures, Prentice Hall, Englewood Cliffs, NJ/London.
3. Kleiber, M. (1989) Incremental Finite Element Modelling in Non-linear Solid Mechanics, Polish Scientific, Warsaw, Ellis Horwood, Chichester.
4. Malvern, L.E. (1969) Introduction to the Mechanics of Continuous Medium, Prentice Hall, Englewood Cliffs, NJ/London.
5. Crisfield, M.A. (1991) Non-linear Finite Element Analysis of Solids and Structures, Wiley, New York.
6. Pinsky, P.M., Ortiz, M., Pister, K.S. (1983) Numerical integration of rate constitutive equations in finite deformations analysis, Computer Methods in Applied Mechanics and Engineering, 40, 137–158.
7. Peric, D., Owen D.R.J., Honnor, M.E. (1985) A model for finite strain elasto-plasticity based on logarithmic strains: Computational issues, Computer Methods in Applied Mechanics and Engineering, 94, 101–118.
8. Simo, J.C., Taylor, R.L. (1985) Consistent tangent operators for rate independent elastoplasticity, Computer Methods in Applied Mechanics and Engineering, 48, 101–118.
9. Gurson, L. (1977) Continuum theory of ductile rupture by void nucleation and growth: Part I – yield criteria and flow rules for porous ductile media, Journal of Engineering Materials and Technology, Transactions of ASME, 99, 2–15.
10. Tvergaard, V. (1982) On localization in ductile materials containing spherical voids, International Journal of Fracture, 18, 237–252.
11. Tvergaard, V. (1981) Influence of voids on shear-band instabilities under plane strain conditions, International Journal of Fracture, 17, 389–407.
12. Simo, J.C., Hughes, T.J.R. (1998) Computational Inelasticity, Springer, New York/London.